THE ASTROPHYSICAL JOURNAL, 513:619–625, 1999 March 10

SPECTROPHOTOMETRIC RESOLUTION OF STELLAR SURFACES WITH MICROLENSING

B. SCOTT GAUDI AND ANDREW GOULD[1]
Ohio State University, Department of Astronomy, Columbus, OH 43210; gaudi@astronomy.ohio-state.edu, gould@astronomy.ohio-state.edu
Received 1998 February 24; accepted 1998 October 19

ABSTRACT

Microlensing is a powerful tool for studying stellar atmospheres, because as the source crosses regions of formally infinite magnification (caustics), the surface of the star is resolved, thereby allowing one to measure the radial intensity profile both photometrically and spectroscopically. However, caustic crossing events are relatively rare and monitoring them requires intensive application of telescope resources. It is therefore essential that the observational parameters needed to accurately measure the intensity profile are quantified. We calculate the expected errors in the recovered radial intensity profile as a function of the unlensed flux, source radius, spatial resolution of the recovered intensity profile, and caustic crossing time for the two principle types of caustics: point-mass and binary lenses. We demonstrate that for both cases there exist simple scaling relations between these parameters and the resultant errors. We find that the error as a function of the spatial resolution of the recovered profile, parameterized by the number of radial bins, increases as $N_R^{3/2}$, considerably faster than the naive $N_R^{1/2}$ expectation. Finally, we discuss the relative advantages of binary caustic-crossing events and point-lens events. Binary events are more common, easier to plan for, and provide more homogeneous information about the stellar atmosphere; however, a subclass of point-mass events with low impact parameters can provide dramatically more information provided that they can be recognized in time to initiate observations.

Subject headings: gravitational lensing — stars: atmospheres

1. INTRODUCTION

Originally proposed by Paczyński (1986) as a method to detect the presence of massive compact objects in the halo of our Galaxy, microlensing has increasingly been recognized as a tool for studying a broad range of astrophysical phenomena. Various applications include detection and characterization of binary and planetary systems (Mao & Paczyński 1991; Gould & Loeb 1992), reconstruction of the stellar mass function down to masses below the hydrogen burning limit (Paczyński 1991; Griest et al. 1991; Gould 1996), measurement of the rotation speed of giants (Gould 1997), measurement of the transverse velocity of galaxies (Gould 1995a), and probing of the central engines of quasars (Gould & Gaudi 1997). Recently, Valls-Gabaud (1994, 1998) and Sasselov (1997) have proposed using microlensing to study stellar atmospheres. Here we analyze this application in detail.

Currently, three collaborations (MACHO, Alcock et al. 1997a; OGLE, Udalski et al. 1997; EROS, Ansari et al. 1996) have ongoing projects that survey the Galactic bulge with roughly nightly sampling in order to detect microlensing events. Over 60 events year^{-1} are being detected. These data are being analyzed in real time, which has allowed MACHO to issue "alerts," notifications of ongoing events detected before the peak. Two follow-up collaborations (PLANET, Albrow et al. 1997, 1998; GMAN, Alcock et al. 1997b) have formed in order to monitor these alerts around the clock with high precision and high temporal sampling with the aim of detecting (and further alerting on) deviations from the standard microlensing light curve, such as would be expected from binary lenses, binary sources, finite sources, and parallax. These deviations are useful in that they can provide additional information about the lens and/or source. In addition, a collaboration has formed to conduct *spectroscopic* monitoring of alerted events in order to study the source stars in detail, and it has observed several events to date (Lennon et al. 1997). Thus the prospect for the real-time detection and monitoring of light-curve anomalies, both photometrically and spectroscopically, is promising.

All gravitational microlenses have caustics, which are defined as the set of points in the source plane where the magnification of a point source is formally infinite. When a finite source crosses a caustic, the gradient of the magnification over the source is large, and therefore different parts of the source are magnified by different amounts. Hence the source is partially resolved. Different parts of the source are resolved at different times during the caustic crossing, and thus by taking a series of measurements during the course of the crossing, one can recover the intensity profile of the source. Several workers realized that finite source effects could be useful for breaking or partially breaking the degeneracy among microlensing event parameters (Gould 1994; Nemiroff & Wickramasinghe 1994; Witt & Mao 1994; Maoz & Gould 1994), and that variations in the surface profile could be exploited to this end (Witt 1995; Loeb & Sasselov 1995; Gould & Welch 1996). However, Valls-Gabaud (1994, 1998), Sasselov (1997), and Heyrovsky, Sasselov, & Loeb (1999) proposed to exploit the same effects for radically different aims. Instead of using finite-source effects to learn more about the lens, they sought to learn more about the source. The basic idea is as follows: imagine that one could separately image different annular rings on the surface of a star. In effect, one would be sampling different depths of the photosphere. Since the temperature varies as a function of depth, the broad spectral energy distribution would change with annulus, with more blue light near the center (greater depths) and more red light near the outer limb (lesser depths). That is, the star would be limb dark-

[1] Alfred P. Sloan Foundation Fellow.

ened, and more so in the blue than the red. Since different spectral lines form at different depths, one would expect that the detailed spectral profile would vary as a function of annular radius. Hence the entire atmosphere could be studied as a function of depth by resolving the two-dimensional (radius and wavelength) spectral profile of the star. Currently, it is only possible to study stellar atmospheres in this way for the Sun and eclipsing binaries. However, since the surface of the source star is partially resolved during a microlensing caustic crossing, one can also probe the atmospheres of the source stars for these types of events.

Both Valls-Gabaud (1994, 1998) and Sasselov (1997) used specific stellar atmosphere models to construct broadband and spectral line brightness profiles, and then used these profiles to predict in detail the variations in the broadband color or equivalent width of specific lines that one would expect during the course of a point-mass microlensing event. Sasselov (1997) and Heyrovsky et al. (1999) also consider the effects of star spots on the microlensing light curve. In addition, they compared their predictions to MACHO Alert event 95-30, a point-mass caustic crossing event for which spectra were taken during the course of the crossing, and for which variations in the optical TiO bands were detected (Alcock et al. 1997b). All of these authors predict that the color and spectral-line variations during the caustic crossing should be significant, and they note that this provides an entirely new method of studying stellar atmospheres.

Although caustic crossing events are, in principle, useful for studying the atmospheres of stars, these events are rare, and they typically last for only about 7 hr (for a giant source). For this method to be successful, it is essential that observers have a clear sense of what can be accomplished with these events, since substantial telescope resources are likely to be expended. To this end we approach this topic from another perspective. We quantify the intrinsic ability of both point-mass and binary lens microlensing caustic crossings to recover the radial variation of the intensity of the star for any arbitrary wavelength, and hence for any spectral line. Specifically, we calculate the fractional error in the recovered intensity profile as a function of the unlensed flux of the source, the duration of the measurements, the size of the telescope, the magnification of the event, and the spatial resolution of the recovered intensity profile. This information will be useful to observers in making rational decisions about which events to follow and what resources are required to address specific questions.

2. FORMALISM

2.1. *Lens Geometry, Magnification, and Caustics*

Microlenses come mostly in two flavors: point lenses and binary lenses. The magnification structure of these two types of lenses is essentially different, so we consider them separately.

The flux of a point source being microlensed by a point lens, F, can be expressed in terms of five parameters: (1) F_0, the unlensed flux of the source; (2) B, the flux of any unresolved background light; (3) t_0, the time of maximum magnification; (4) β, the impact parameter of the event; and (5) t_e, the timescale of the event. These are related by $F = F_0 A(t) + B$, where $A(t)$ is the magnification, which is itself a function of the parameters t_0, t_e, and β, and is given by

$$A[x(t)] = \frac{x^2 + 2}{x(x^2 + 4)^{1/2}}, \quad x(t) = \left[\beta^2 + \frac{(t - t_0)^2}{t_e^2}\right]^{1/2}. \quad (1)$$

Here x and β are in units of the Einstein ring radius, R_E, given by

$$R_E = \frac{[4GMD_{OL}(1 - D_{OL}/D_{OS})]^{1/2}}{c^2}, \quad (2)$$

where M is the mass of the lens, and D_{OL} and D_{OS} are the distances to the lens and to the source, respectively. The timescale is related to the Einstein ring radius by $t_e = R_E/v$, where v is the transverse speed of the lens relative to the observer-source line of sight. Note that for $x \ll 1$, $A(x) \simeq x^{-1}$, and that the magnification therefore diverges for a point source. Thus the point $x = 0$ corresponds to the caustic for the point-lens case. Consider a source of radius R_*. The radius of this star, projected onto the lens plane in units of R_E, is given by

$$\rho = \frac{R_*}{R_E}\frac{D_{OL}}{D_{OS}}. \quad (3)$$

For $M = 0.3\ M_\odot$, $D_{OL}/D_{OS} = 0.75$, $D_{OS} = 8$ kpc, $R_* = 10\ R_\odot$, and $\rho \simeq 0.02$. For a source of this size, equation (1) remains valid for the majority of the event. However, when the lens comes within $\sim 2\rho$ of the source, i.e., for events with $\beta \lesssim 2\rho$, the magnification deviates from equation (1) and the finite size of the source must be considered. The timescale for this deviation is roughly the crossing time for the source, $t_{cross} = \rho t_e \simeq 7(R_*/10\ R_\odot)$ hr for typical bulge events. For these events the source parameter ρ enters into the calculation of the magnification. The probability of such an event is $\sim\langle\rho\rangle$, where $\langle\rho\rangle$ is the average radius of the source stars being monitored. If 100 giant source events were detected during 1 yr, then the lens would transit the source for about 5 events, and these would exhibit finite-source deviations (Gould 1995b).

The magnification of a point source being lensed by a binary depends on the same parameters as the point lens, t_0, t_e, and β, along with the additional parameters b (the separation of the lenses in units of R_E), q (the mass ratio of the lenses), and θ (the angle between the axis of the binary and the trajectory). Unfortunately, the dependence of the magnification on these parameters in the general case has no analytic form. Since the method of determining the magnification in the general case has been described elsewhere (see, e.g., Witt & Mao 1995), and since we are only interested in caustic crossings, we will employ a simplified formalism for these crossings. For nearly equal mass binary lenses, the caustics are composed of curved lines (called folds) whose extent is of order the Einstein ring radius. Thus the probability of encountering a fold caustic during a binary-lens event is almost unity. For a point source, the excess magnification near the fold caustic is approximately $A \propto x^{-1/2}$ (Schneider, Ehlers, & Falco 1992), where x is the distance from the caustic, and the magnification diverges at $x = 0$ (at the caustic). For a finite source of radius ρ, the magnification deviates from this form for distances $x \lesssim 2\rho$, and the finite size of the source must be considered. Binary lenses also have cusps, points where two fold caustics merge, and the magnification structure near a fold is quite different from that near a cusp. In particular, it cannot be described by the same equations. While the probability of encountering a fold caustic is nearly unity, the probability

of encountering a cusp is $\sim N\rho$, where N is the number of cusps. For typical binary lenses $N = 6$, and thus the probability is $\sim 20\%$. If 100 events were discovered toward the bulge per year, and 5% of these were binaries, we would expect only one cusp crossing per year, while we would expect five events with fold crossings. Hence we will consider only fold crossings here.

Before continuing to the next section, where we consider the magnification one expects when a finite source crosses the two types of caustics considered above, we include a brief discussion concerning notation. Note that there are two characteristic scales in this problem, R_E and ρ, which are related by equation (3). Either of these could be used as our fiducial scale. For definiteness, we choose to scale all quantities by R_E. For the remainder of the discussion, we will also assume that $t = 0$ is the time when the center of the source crosses (or comes closest to) the caustic. For the point-mass case, this simply means setting $t_0 = 0$. Finally, for the binary lens the caustic crossings come in pairs. Throughout we will be referring to the second caustic crossing (since it is this crossing that can be predicted; see § 5) when the source is moving from the inside of the caustic structure to the outside.

2.2. *Extended Sources*

The magnification of an extended source is given by

$$A_{es}(t) = \frac{\int d^2r A(t; \mathbf{r}) I(\mathbf{r})}{\int d^2r I(\mathbf{r})}, \tag{4}$$

where $I(\mathbf{r})$ is the intensity profile of the source, A is the magnification of a point source at $\mathbf{r}$, and the integral is over the area of the source. The numerator and denominator are, respectively, the lensed and unlensed flux of the source. Assuming that the intensity profile has azimuthal symmetry, and using polar coordinates, this becomes

$$A_{es}(t) = \frac{\int_0^\rho dr r I(r) \mathscr{A}(t; r)}{\int_0^\rho dr r I(r)}, \tag{5}$$

where $\mathscr{A}(r)$ is the angle-averaged magnification function

$$\mathscr{A}(r) \equiv \frac{1}{2\pi} \int_0^{2\pi} A(r, \theta) d\theta . \tag{6}$$

This definition is useful because the magnification geometry of the lens is entirely isolated in this function. Once the function has been calculated, it can be convolved with any source intensity profile to give the total magnification A_{es}. Furthermore, it is the shape of this function that determines how well one can resolve the source; i.e., if $\mathscr{A}$ is highly peaked at a particular value of r, then the majority of the lensed flux will be coming from a small range of radii near r, and therefore the lens is resolving the source.

2.3. *Angle-averaged Magnification Functions*

For both fold and point caustic crossings, the approximate form of the function $\mathscr{A}$ can be calculated analytically. When a source crosses a fold caustic, two images appear or disappear. For typical total binary-lens mass, the size of the source, ρ, is considerably smaller than the Einstein ring radius of the lens, $\rho \ll 1$, and thus the magnification of the other three images changes very little as the source crosses the caustic. Also, the curvature of the caustic is typically very small across the source. In this regime the magnification in the vicinity of the fold caustic can be approximated by (Schneider et al. 1992)

$$A(x) = A_0 + \left(\frac{b_0}{R_E}\right)^{1/2} x^{-1/2}, \quad x > 0 \text{ (inside the caustic)}, \tag{7}$$

where A_0 is the total magnification of the three unrelated images, x is the distance to the caustic, and b_0 describes the scale of the caustic. For approximately equal mass binaries, $b_0 \sim R_E$. For $x < 0$ (outside the caustic), $A(x) = A_0$. Defining $z = x/r$, where x is now the distance from the center of the source to the caustic, and setting $b_0 = R_E$, the angle-averaged magnification function is

$$\mathscr{A}(r) = A_0 + r^{-1/2} j(z), \tag{8}$$

where

$$j(z) = \begin{cases} 0 & \text{if } z < -1, \\ \dfrac{2^{1/2}}{\pi} K\left[\left(\dfrac{1+z}{2}\right)^{1/2}\right] & \text{if } |z| < 1, \\ \dfrac{2}{\pi}(1+z)^{-1/2} K\left[\left(\dfrac{2}{1+z}\right)^{1/2}\right] & \text{if } z > 1. \end{cases} \tag{9}$$

Here K is the complete elliptic integral of the first kind. Figure 1 shows $\mathscr{A}(r/\rho)$ versus r/ρ for $A_0 = 0$, and $\rho = 1$, and $x = -t/t_e = z\rho = 5/3\rho$, ρ, $\frac{2}{3}\rho$, $\frac{1}{3}\rho$, 0, $-\frac{1}{3}\rho$, and $-\frac{2}{3}\rho$. For $x = -t/t_e > \rho$ (when the source is entirely contained within the caustic), the gradient of the magnification across the face of the source is small, and furthermore $\mathscr{A}(r/\rho)$ has no maximum. This implies that these times are not useful for resolving the source. For $0 < x = -t/t_e < \rho$, $\mathscr{A}(r/\rho)$ shows a sharp peak at $r = x$, and thus the source is being resolved. However, other annuli are being significantly magnified and

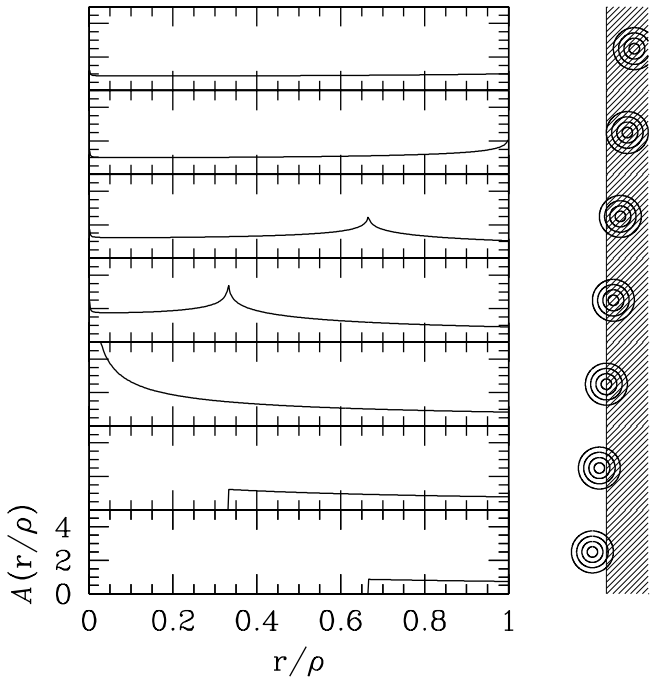

FIG. 1.—Angle-averaged magnification, $\mathscr{A}$, as a function of the radius in units of the source radius r/ρ for the fold caustic case for seven different times, $x = -t/t_e = 5/3\rho$ (*top*), ρ, $\frac{2}{3}\rho$, $\frac{1}{3}\rho$, 0, $-\frac{1}{3}\rho$, and $-\frac{2}{3}\rho$ (*bottom*). The associated geometry is shown to the right of each panel. We have set the magnification not associated with the caustic to zero, and have taken $\rho = 1.0$. For other source radii, $\mathscr{A}$ scales as $\rho^{-1/2}$.

are thus contributing significantly to the total light, and therefore the resolution will be degraded somewhat. By contrast, for $-\rho < x = -t/t_e < 0$ and in the limit $A_0 \to 0$, only those annuli that have just crossed the caustic contribute to the total light. It is therefore these times that are most useful for resolving the source.

For a source of uniform brightness, the total magnification is (Schneider & Weiss 1987)

$$A_{\rm es}(r) = A_0 + r^{-1/2}\mathcal{J}(z)\,, \tag{10}$$

where

$$\mathcal{J}(z) = 0\,, \qquad \text{if } z < -1\,; \tag{11a}$$

$$\mathcal{J}(z) = \frac{2^{5/2}}{3\pi}\left\{(1-z)K\left[\left(\frac{1+z}{2}\right)^{1/2}\right] + 2zE\left[\left(\frac{1+z}{2}\right)^{1/2}\right]\right\}, \qquad \text{if } |z| < 1\,; \tag{11b}$$

$$\mathcal{J}(z) = \frac{8}{3\pi}(1+z)^{1/2}\left\{zE\left[\left(\frac{2}{1+z}\right)^{1/2}\right] - (z-1)K\left[\left(\frac{2}{1+z}\right)^{1/2}\right]\right\}, \qquad \text{if } |z| < 1\,. \tag{11c}$$

and E is the complete elliptic integral of the second kind. Note that in equations (8) and (10) the dependences on z and r are separable for $A_0 = 0$. This implies that for a fixed value of z both $\mathcal{A}$ and $A_{\rm es}$ scale simply as $\rho^{-1/2}$.

We now turn to the point lens case. When the separation between the lens and the source is much smaller than the Einstein ring radius, $x \ll R_{\rm E}$, the magnification can be approximated by

$$A(x) = x^{-1}\,. \tag{12}$$

The angle-averaged magnification function is then

$$\mathcal{A}(r) = r^{-1}b(z)\,, \tag{13}$$

where

$$b(z) = \frac{2}{\pi}(1+z)^{-1}K\left[\frac{4z}{(1+z)^2}\right], \tag{14}$$

and K is the complete elliptic integral of the first kind. Figure 2 shows $\mathcal{A}(r/\rho)$ versus r/ρ for $\rho = 1$ and trajectories with $x = (t^2/t_e^2 + \beta^2)^{1/2}$, for impact parameters $\beta = 0$ (*solid lines*) and $\beta = 0.5\rho$ (*dashed lines*), and $t/t_e = -\rho$, $-\frac{2}{3}\rho$, $-\frac{1}{3}\rho$, 0, $\frac{1}{3}\rho$, $\frac{2}{3}\rho$, and ρ. Here $\mathcal{A}$ achieves a local maximum whenever $r = x$, which implies that these radii are being partially resolved at these times. Unfortunately, for any impact parameter $\beta > 0$, there is a range of source radii at which $\mathcal{A}$ is never at a maximum, and those for which $r < \beta$. These radii are not resolved during the caustic crossing, and thus very little information about the radial intensity profile will be gained for this range of source radii.

The total magnification for a source of uniform brightness is (Schneider et al. 1992)

$$A_{\rm es}(r) = r^{-1}\mathcal{B}(z)\,, \tag{15}$$

where

$$\mathcal{B}(z) = \begin{cases} \dfrac{4}{\pi}E(z) & \text{if } z \le 1\,, \\ \dfrac{4}{\pi}z[E(1/z) - (1-z^{-2})K(1/z)] & \text{if } z \ge 1\,. \end{cases} \tag{16}$$

As in the fold case, the dependences on z and r in equations (13) and (15) are separable. Thus for a fixed value of z, $\mathcal{A}$ and $A_{\rm es}$ scale as ρ^{-1}.

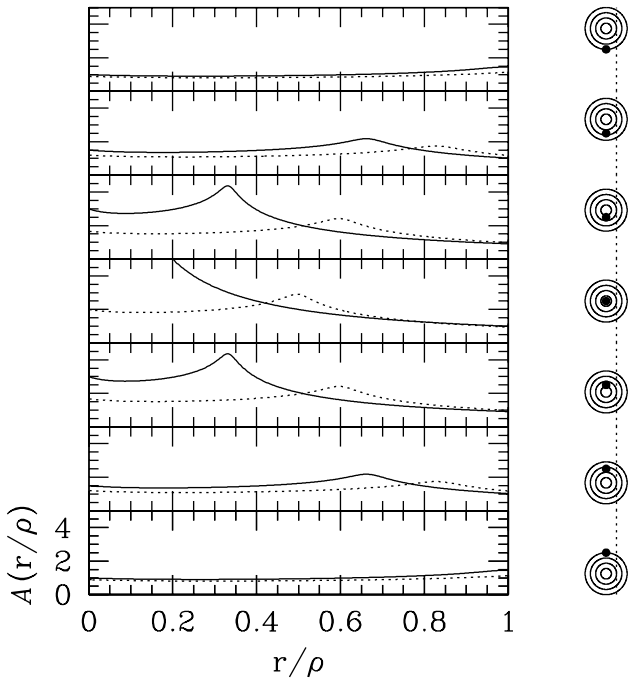

FIG. 2.—Angle-averaged magnification, $\mathcal{A}$, as a function of the radius in units of the source radius r/ρ for the point caustic case for seven different times, $t/t_e = -\rho$ (*top*), $-\frac{2}{3}\rho$, $-\frac{1}{3}\rho$, 0, $\frac{1}{3}\rho$, $\frac{2}{3}\rho$, and ρ (*bottom*), and two different trajectories, $\beta = 0$ (*solid lines*) and $\beta = 0.5\rho$ (*dashed lines*). The associated geometry is shown to the right of each panel. We have taken $\rho = 1.0$. For other source radii, $\mathcal{A}$ scales as ρ^{-1}.

3. ERROR ANALYSIS

The flux measured from a star of finite size being lensed is $F(r) = A_{\rm es}F_0 + B$, where the general form of $A_{\rm es}$ is given in equation (4). For most caustic crossing events, the magnification is high and $A_{\rm es}F_0 \gg B$; thus we will henceforth use the approximation that $B = 0$. Consider a star divided up into N_r radial bins, each located at r_i. Defining Δr_i as the width of this bin, the flux of the star is given by

$$F(t) = \sum_i^{N_r} 2\mathcal{A}(r_i)I(r_i)r_i\,\Delta r_i\,, \tag{17}$$

where $\mathcal{A}$ is the angle-averaged magnification in bin i. For the case of a large number of bins, or $\Delta r_i \ll \rho$, the magnification in each bin is well approximated by equations (8) and (13). For a small number of bins, however, these forms are not good approximations, and one should use the total magnification in each bin, which can be obtained by either integrating equations (8) and (13) over the radii of the bin, or, equivalently, by using equations (10) and (15) and subtracting the flux within the inner radius of the bin from the flux within the outer radius of the bin and dividing by the area of the annulus. In practice, the latter is simpler. The parameters one would like to recover are $I(r_i)$, the mean intensity in bin i for a certain wavelength. In order to do this, however, one must first know $\mathcal{A}(r_i)$, which implies knowing the parameters ρ, β, t_e, and t_0 for the point-lens case, and the additional parameters θ, b, and q for the binary case. In principle, one could determine these param-

eters entirely within the context of the spectrophotometric measurements. However, variations in the seeing and extinction make this difficult. Fortunately, this is not a significant hindrance because independent broadband measurements can be used to constrain these parameters. Since the follow-up collaborations already monitor these events and, in one case, have already used broadband measurements to constrain these parameters *and* measure the limb darkening of the source star (Albrow et al. 1999), this should not be a problem in practice, although it does imply that the spectroscopic and photometric follow-up collaborations should closely coordinate their efforts. Now suppose that a series of spectrophotometric measurements $F(t_k)$ are made at times t_k, with uncertainties σ_k, and these measurements are fitted to equation (17). The parameters of this fit are I_i, and the covariance matrix of the errors in these parameters is given by c_{ij}, where

$$c = b^{-1}, \quad b_{ij} = \sum_k \sigma_k^{-2} \frac{\partial F(t_k)}{\partial I_i} \frac{\partial F(t_k)}{\partial I_j}, \tag{18}$$

and $\partial F(t_k)/\partial I_i = 2\mathscr{A}(r_i) r_i \Delta r_i$. The variances in the parameters are then the diagonal elements of c_{ij}, and thus the fractional error in each parameter is $\delta I_i/I_i = (c_{ii})^{1/2}/I_i$. Assuming photon-limited precision, the fractional errors scale as the square root of the total number of photons received, which in turn scales as $(A_{\rm es} F_0)^{1/2}$. From equation (10), $A_{\rm es} \propto \rho^{-1}$ for the point caustic, and from equation (15) $A_{\rm es} \propto \rho^{-1/2}$ for the fold caustic. Let γ be the rate at which a telescope receives photons from the unmagnified star in a certain spectral range, and assume that measurements are made continuously during a source-radius crossing time, $t_{\rm cross}$. Then the square root of the total number of photons scales as $\rho^{-\nu}(\gamma t_{\rm cross})^{1/2}$, where $\nu = 1/2$ for the point caustic and $\nu = 1/4$ for the fold caustic. The fractional errors will also depend on the spatial resolution of the recovered intensity profile N_r. Assuming Poisson statistics and no correlations between the parameters I_i, one would expect the fractional errors in I_i to scale simply as $N_r^{1/2}$. However, we find that the parameters I_i are correlated, and the errors in fact scale approximately as $N_r^{3/2}$. We justify this assertion in the next section. Taking these scalings out of c_{ii}, we have

$$\frac{\delta I_i}{I_i} = N_r^{3/2} (\gamma t_{\rm cross})^{-1/2} \rho^{\nu} (\tilde{c}_{i,i})^{1/2}, \tag{19}$$

where $(\tilde{c}_{ii})^{1/2}$ is the normalized fractional error for $N_r = 1$, $\rho = 1$, and $\gamma t_{\rm cross} = 1$. The specific form of $(\tilde{c}_{i,i})^{1/2}$ will depend on the details of the caustic encounter and will therefore vary on an event-by-event basis. In the next section we consider specific cases and evaluate $(\tilde{c}_{ii})^{1/2}$ directly.

4. RESULTS

4.1. *Scaling with Number of Radial Bins*

In order to justify the assertion that the errors scale as $N_r^{3/2}$, we consider a specific example for each caustic case. For the point case we consider an event with impact parameter $\beta = 0$, and we assume that this event is observed from $t/t_e = 0$ to $t/t_e = \rho$, i.e., for one source crossing time. We then evaluate the normalized error, $(\tilde{c}_{i,i})^{1/2}$, for this event as a function r_i, the radius of the bin, for different values of N_r. This is shown in Figure 3*a* for $N_r = 10, 20, 40$. If the errors scaled exactly as $N_r^{3/2}$, these curves would be indistinguishable. In fact, the normalized errors decrease slightly for larger N_r, which indicates that the errors do not increase quite as fast as $N_r^{3/2}$, although this depends on r_i. For the fold case, we assume that the event is observed from $x = -t/t_e = 0$, when the center crosses the caustic, until $x = -t/t_e = -\rho$, when the source moves completely outside the caustic. In Figure 3*b*, we show $(\tilde{c}_{ii})^{1/2}$ for $N_r = 10, 20, 40$. Here the scaling is nearly perfect. We will henceforth assume that the scaling is perfect for both cases, and therefore that $\tilde{c}_{ii}$ has no dependence on N_r.

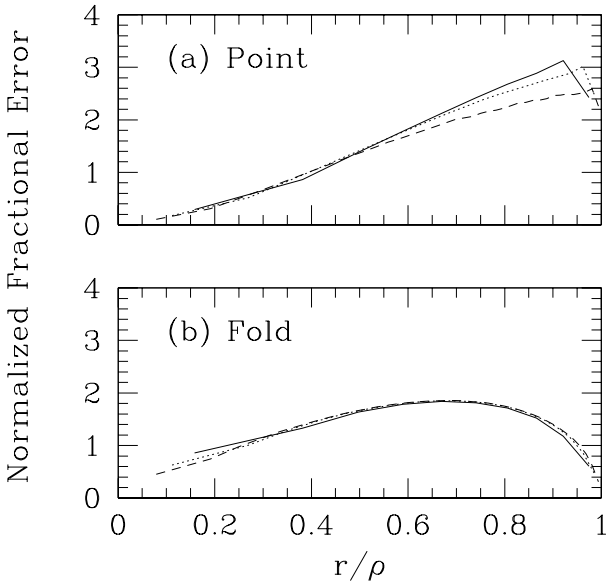

FIG. 3.—(*a*) Normalized fractional error in the recovered intensity profile ($\delta I/I$) as a function of the radius in units of the source radius r/ρ for the point caustic. Each line corresponds to a different number of radial bins, N_r, in the recovered intensity profile, $N_r = 10$ (*solid line*), 20 (*dotted line*), and 40 (*dashed line*). (*b*) Same as (*a*) except for the fold caustic.

4.2. *Fractional Errors*

In order to evaluate the fractional errors explicitly, we adopt some fiducial parameters. For a giant in the bulge and a typical microlensing event, $\rho \sim 0.02$, and we assume that observations are taken continuously for a time, $t_{\rm cross} \sim 7$ hr. We use $N_r = 10$ for our fiducial number of radial bins, and for the moment we assume a uniformly bright source, since this is the most general way to quantify the error in a model-independent way. In the next section, we consider a source with limb darkening. The fractional error in the intensity profile for these parameters is

$$\frac{\delta I_i}{I_i} = \left(\frac{\delta I_i}{I_i}\right)_0 \left(\frac{\rho}{0.02}\right)^{\nu} \left(\frac{t_{\rm cross}}{7\ {\rm hr}}\right)^{-1/2} \left(\frac{\gamma}{0.4\ {\rm s}^{-1}}\right)^{-1/2} \left(\frac{N_r}{10}\right)^{3/2}, \tag{20}$$

where $\nu = \frac{1}{2}$ for the point caustic and $\nu = \frac{1}{4}$ for the fold caustic, and $\gamma = 0.4\ {\rm s}^{-1}$ is approximately the flux of photons per spectral resolution element from a star with $V = 17$ that can be acquired with a 2 m telescope and a spectrograph with 1 Å resolution. In Figure 4*a* we show $(\delta I/I)_0$ as a function of r_i for the point-lens case, $t/t_e = 0$ to ρ, and for four different impact parameters, $\beta/\rho = 0$, 0.25, 0.50, and 0.75 (*solid*, *dotted*, *short-dashed*, and *long-dashed lines*). It is clear from this diagram that for $r > \beta$ the fractional error is small, $\lesssim 10\%$. One could, in principle,

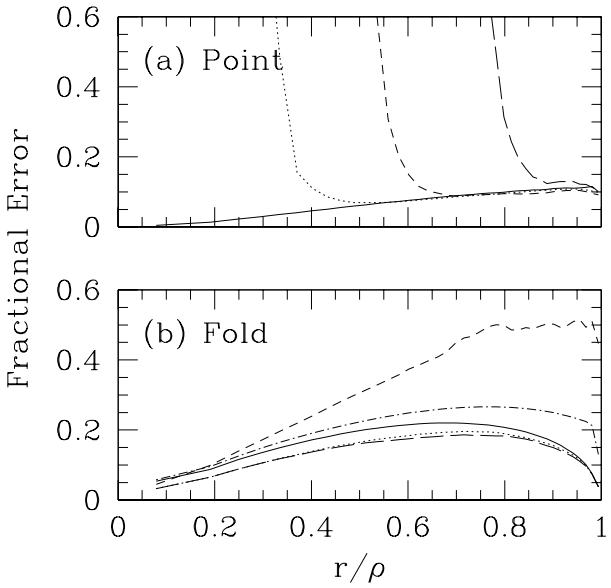

FIG. 4.—Fractional error in the recovered intensity profile ($\delta I/I$) as a function of the radius in units of the source radius r/ρ for the fiducial parameters: $N_r = 10$ (number of radial bins in the recovered intensity profile), $\gamma = 0.4\ \mathrm{s}^{-1}$ (unlensed flux of star), $t_{\mathrm{cross}} = 7$ hr (crossing time of star) and $\rho = 0.02$. (*a*) Errors for the point caustic for t/t_e from 0 to ρ and four different values of the impact parameter, $\beta/\rho = 0$ (*solid line*), 0.25 (*dotted line*), 0.5 (*short-dashed line*), and 0.75 (*long-dashed line*). (*b*) Errors for the fold caustic for four different trajectories: $x = -t/t_e$ from 0 to $-\rho$ (*solid line*), ρ to 0 (*short-dashed line*), ρ to $-\rho$ (*dotted line*), and 2ρ to $-\rho$ (*long-dashed line*). For these curves we have set the magnification not associated with the caustic to zero ($A_0 = 0$). We also show the fractional error for the case $A_0 = 1$ and $x = -t/t_e$ from 0 to $-\rho$ (*dash-dotted line*).

improve the fractional error by a factor of $2^{1/2}$ by observing from $-\rho < t/t_e < \rho$, i.e., for two source crossings. However, this will prove difficult in practice (see § 5). While the errors are small for $r > \beta$, there is almost no information for radii $r < \beta$, as expected, since the lens is not passing over this region of the star. In Figure 4*b* we show $(\delta I/I)_0$ as a function of r_i for the fold caustic, with $A_0 = 0$ and four different cases. The short-dashed line corresponds to measurements taken from $x = -t/t_e = \rho$ to $x = 0$, which is one crossing time from when the edge of the source first crosses the caustic to when the source is exactly centered on the caustic, i.e., the first half of the caustic crossing. The solid line corresponds to $x = 0$ to $x = -t/t_e = -\rho$ (the second half of the caustic crossing); the dotted line corresponds to $x = -t/t_e = \rho$ to $x = -t/t_e = -\rho$ (the entire caustic crossing); and the long-dashed line corresponds to $x = -t/t_e = 2\rho$ to $x = -t/t_e = -\rho$. From this figure one learns three things. First, the errors are reasonable, $\delta I/I \lesssim 20\%$ for typical parameters. Second, the times immediately after the center of the source crosses the caustic are the most crucial for recovering the intensity profile accurately. Finally, it is only the times just before until just after the caustic crossing that are useful for resolving the source. We also show the errors for the case that $A_0 = 1$ (*dash-dotted line*). Clearly, the magnification of the images not associated with the caustic does not greatly affect the resultant errors.

4.3. *Effects of Limb Darkening*

In this section we examine the effect limb darkening has on the fractional error in the recovered intensity profile. We can anticipate that limb darkening will serve to increase the errors in the outer annuli relative to the constant surface brightness case because there will be fewer photons coming from outer annuli, and thus the errors will be larger. For the inner annuli, the fractional errors will be smaller compared to the constant surface brightness case because the source is, in essence, more compact, and thus the net magnification will be larger, and therefore the errors smaller.

To quantify this effect, we apply the same formalism as in § 3, except we adopt the following parameterization of the surface brightness as a function of radius:

$$\frac{I(r)}{I(0)} = 1 - \kappa_1 Y - \kappa_2 Y^2\,, \quad Y = 1 - \left(1 - \frac{r^2}{\rho^2}\right)^{1/2}\,, \quad (21)$$

where κ_1 and κ_2 are the limb-darkening coefficients. We adopt the coefficients for a cool (4500 K) giant ($\log g = 1.5$) of solar metallicity from Manduca, Bell, & Gustafsson (1977) and Manduca (1979). These are $\kappa_1 = 0.798$, 0.567, and 0.139, and $\kappa_2 = -0.007$, 0.114, 0.259 for the V, I, and K bands, respectively. Since stars are less limb darkened in the infrared, the results for the K band will be the most similar to the uniform surface brightness case, while those for V will be least similar. The results for the same fiducial parameters used in § 4.2 ($\rho = 0.02$, $t_{\mathrm{cross}} = 7$ hr, $\gamma = 0.4\ \mathrm{s}^{-1}$, and $N_r = 10$) are shown in Figure 5 along with the uniform surface brightness case. For the point-caustic case (Fig. 5*a*), we have used a trajectory with $\beta = 0$ and assumed that observations are taken for $0 < t/t_e < \rho$. For larger values of β, the fractional errors will deviate more dramatically from the uniform surface brightness case, since for large values of β only the outer annuli are being effectively resolved, and it is these annuli that are affected most by limb darkening. For the fold caustic case (Fig. 5*b*), we have assumed $-\rho < x = -t/t_e < \rho$. As expected, for both the point-caustic and fold-caustic cases the fractional errors are somewhat larger than for the uniform source at larger radii and somewhat smaller at smaller radii. Also, the differences

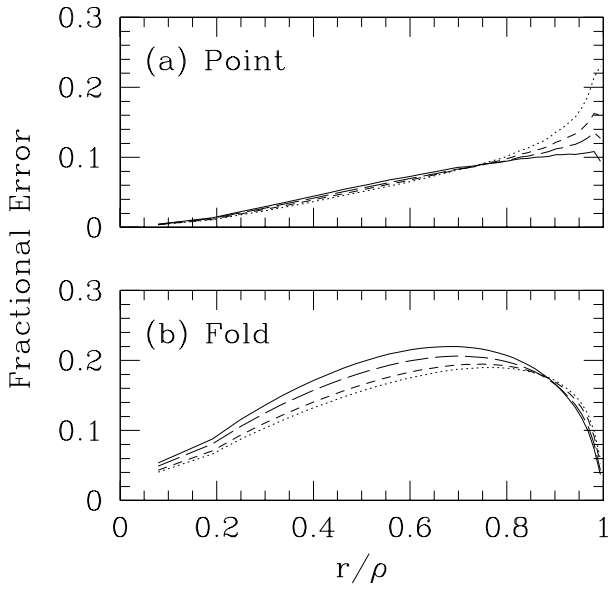

FIG. 5.—(*a*) Fractional error in the recovered intensity profile ($\delta I/I$) as a function of the radius in units of the source radius r/ρ for the point caustic, a uniform source (*solid line*), and a limb-darkened source as appropriate for the broad bands V (*dotted line*), I (*short-dashed line*), and K (*long-dashed line*). (*b*) Same as (*a*) except for the fold caustic. For both (*a*) and (*b*) we have assumed the same fiducial parameters as the solid lines in Fig. 4.

between the uniform source and limb-darkened source decrease for longer wavelengths. In general, however, for both the point and fold caustics the differences between uniform and limb-darkened sources is modest. For fold caustics the effect is $\lesssim 25\%$ over the entire range of radii. For point caustics the effect is small over most of the star, but the error can more than double at the very limb of the star when observed in the V band, the bluest color considered here.

5. DISCUSSION

While both point-mass lenses and binary lenses can in principle be used to resolve the two-dimensional (radial and spectral) profile of a star, binary lenses are substantially easier to use. First, for a binary lens one always has warning of the second caustic crossing. When the source crosses the caustic the first time it is suddenly magnified by a factor of $\rho^{-1/2} \sim 7$, and hence is easily recognized. The second crossing can then be expected in several days to several weeks. Intensive photometric monitoring (now routinely undertaken by PLANET and GMAN) can then be analyzed to make a more precise prediction. From Figure 4*b* it is clear that the most useful portion of the second caustic crossing is the final $\sim 70\%$ of the time that the source actually straddles the caustic. The onset of this optimal period can be judged extremely accurately if photometric monitoring is proceeding simultaneously, and judged reasonably accurately even 1 day in advance. By contrast, there is no way to guarantee a priori that a point-mass caustic crossing will occur, because one does not know the size of the Einstein ring projected onto the source plane beforehand, and hence one does not know ρ. Using optical photometry alone, one can "predict" a source crossing only at about the time it begins. Using optical/infrared photometry, it could be predicted at $r \sim 1.5\ \rho$ (Gould & Welch 1996), but this would leave only a few hours' warning.

Second, fold caustics generically provide information about the entire radial profile of the star, while point caustics provide information only for annuli of the star that are greater than the impact parameter β (see Fig. 4). Again, it is virtually impossible to predict in advance for which events $\beta \ll \rho$ (and hence for which events one can resolve essentially the whole star), although once the peak occurred, these events could be recognized provided that the star was being monitored photometrically. In any event, of all point-caustic transits, only a fraction, β/ρ, have impact parameters smaller than β.

Third, binary-lens events are probably more common than point-mass caustic crossings. The fraction of events with binary-caustic crossings has not yet been established empirically, but 5% appears to be a plausible estimate. The fraction of point-mass caustic crossings is $\langle\rho\rangle$, but by the argument of the previous paragraph about only half of these are really useful. The mean radius of a giant is $R \sim 22\ R_\odot$ (Gould 1995b), about 2.2 times larger than the fiducial value used in equation (20). Thus the fraction of events with useful point-mass caustic crossings is $\sim 0.5\langle\rho\rangle \sim 2\%$.

On the other hand, as shown by Figure 4, over the range probed by the point lens ($r < \beta$), the point-lens errors are less than half as large as those of the binary. This advantage diminishes as $\rho^{-1/4}$ for larger stars, but it is still substantial for most giants. The problem of recognizing events with $\beta \ll \rho$ sufficiently early to permit spectroscopic monitoring is formidable. However, if they can be monitored beginning at their peak, they are the best events to follow.

This work was supported in part by grant AST 94-20746 from the NSF.

REFERENCES

Albrow, M., et al. 1997, in Variable Stars and the Astrophysical Returns of Microlensing Surveys, ed. R. Ferlet, J.-P. Maillard, & B. Raban (Gif-sur-Yvette: Editions Frontières), 135
———. 1998, ApJ, 509, 687
———. 1999, ApJ, in press
Alcock, C., et al. 1997a, ApJ, 479, 119
———. 1997b, ApJ, 491, 436
Ansari, R., et al. 1996, A&A, 314, 94
Gould, A. 1994, ApJ, 421, L71
———. 1995a, ApJ, 444, 556
———. 1995b, ApJ, 447, 491
———. 1996, PASP, 108, 465
———. 1997, ApJ, 483, 98
Gould, A., & Gaudi, B. S. 1997, ApJ, 486, 687
Gould, A., & Loeb, A. 1992, ApJ, 396, 104
Gould, A., & Welch, D. 1996, ApJ, 464, 212
Griest, K., et al. 1991, ApJ, 372, 79
Heyrovsky, D., Sasselov, D., & Loeb, A. 1999, in preparation
Lennon, D. J., et al. 1997, The Messenger, 90, 30L
Loeb, A., & Sasselov, D. 1995, ApJ, 449, 33L
Manduca, A. 1979, A&AS, 36, 411
Manduca, A., Bell, R. A., & Gustafsson, B. 1977, A&A, 61, 809
Mao, S., & Paczyński, B. 1991, ApJ, 374, 37
Maoz, D., & Gould, A. 1994, ApJ, 425, L67
Nemiroff, R. J., & Wickramasinghe, W. A. D. T. 1994, ApJ, 424, L21
Paczyński, B. 1986, ApJ, 304, 1
———. 1991, ApJ, 371, 63
Sasselov, D. 1997, in Variable Stars and the Astrophysical Returns of Microlensing Surveys, ed. R. Ferlet, J.-P. Maillard, & B. Raban (Gif-sur-Yvette: Editions Frontières), 141
Schneider, P., Ehlers, J., & Falco, E. E. 1992, Gravitational Lenses (Berlin: Springer)
Schneider, P., & Weiss, A. 1987, A&A, 171, 49
Udalski, A., et al. 1997, Acta Astron., 47, 169
Valls-Gabaud, D. 1994, in Large-Scale Structures of the Universe, ed. J. Mucket et al. (Singapore: World Scientific), 326
———. 1998, MNRAS, 294, 747
Witt, H. 1995, ApJ, 449, 42
Witt, H., & Mao, S. 1994, ApJ, 430, 505
———. 1995, ApJ, 447, L105